Variable-Temperature Fourier Transform Infrared Studies of Matrix–Nanofiller Interactions in Amorphous Polyamide/Layered Silicate Nanocomposites

Xingui Zhang, Leslie S. Loo

School of Chemical and Biomedical Engineering, Nanyang Technological University, Singapore 637459, Singapore

Received 27 October 2011; accepted 9 December 2011
DOI 10.1002/app.36659
Published online in Wiley Online Library (wileyonlinelibrary.com).

ABSTRACT: Variable-temperature Fourier transform infrared spectroscopy was used to investigate matrix–nanofiller interactions in amorphous semiaromatic polyamide/layered silicate nanocomposites prepared by melt intercalation. The types of polymer–nanofiller interactions were found to be strongly dependent on the nature of the polymer matrix and the surfactant-modified layered silicate. Improved compatibility resulted when hydrogen-bonding interactions occurred between the surfactant and polymer chains. The presence of surfactants with phenyl groups also led to a more stable molecular structure of the polymer matrix because of the enhanced resonance effect between aromatic groups. Si—O stretching vibrations in the layered silicate shifted to lower wavenumbers with increasing temperature; this indicated the presence of weaker polymer-layered silicate interactions. The results of this study demonstrate that for the polymer nanocomposites prepared by melting intercalation, more important interfacial interactions existed between the polymer and the surfactant. © 2012 Wiley Periodicals, Inc. J Appl Polym Sci 000: 000–000, 2012

Key words: nanocomposites; nylon; FT-IR

Recent interest in polymer/layered silicate nanocomposites has been motivated by the potential of achieving enhanced properties at lower nanofiller loadings compared to higher loadings for conventional micrometer-size fillers.[1,2] For instance, the addition of 5 wt % montmorillonite (MMT) nanoclay to polyamide 6 increased its Young's modulus[3,4] and heat distortion temperature[5] and also improved its barrier properties.[6] Because only a small amount of inorganic material is needed to produce these desired characteristics, the degree of clay dispersion and the polymer–nanoclay interaction have been found to be critical in determining the final properties of the nanocomposites.[2] Usually, the exfoliation of nanoclay leads to a large number of particles with a high surface area, with the possibility of much more matrix-reinforcement interactions than in conventional composites.[7] However, most conclusions or assumptions about the reinforcing mechanism of the polymer/clay nanocomposites have not been based on direct microevidence but on macroproperties, and the effects of interfacial interactions are not well understood.[8]

Correspondence to: L. S. Loo (ssloo@ntu.edu.sg).
Contract grant sponsor: Nanyang Technological University.

Fourier transform infrared (FTIR) spectroscopy and variable-temperature Fourier transform infrared (VT–FTIR) spectroscopy are powerful methods for studying interfacial interactions at the molecular level. Infrared absorptions are very sensitive to interactions between different species.[9] One important type of intermolecular interaction in polymer nanocomposites is hydrogen bonding. FTIR spectroscopy has been used widely to characterize hydrogen bonding and its thermal motion at the molecular level.[8,10,11] Although the bond energies of hydrogen bonds are weaker (15–40 kJ/mol) than those of covalent bonds (on the order of 400 kJ/mol), changes in the environment of the hydrogen-bonded species can result in appreciable peak shifts and intensity changes in the vibrational spectra of the polymer.[12] In previous studies using VT–FTIR spectroscopy, it has been reported that for polymer/organoclay nanocomposites based on polycarbonate[13] and poly (ethylene-*ran*-vinyl acetate-*ran*-vinyl alcohol),[9] there were changes in the polymer spectra when the organoclay contained surfactants with a hydroxyl group. The changes were attributed to hydrogen bonding between the polymer and hydroxyl group of the surfactant. However, because of the small amount of surfactant present in the nanocomposites, it was not possible to detect corresponding changes in the infrared spectra of the surfactant.

Many studies of semicrystalline polyamide (e.g., polyamide 6, polyamide 66) nanocomposites also

showed changes in the peak positions and band shapes of the amide modes (e.g., N—H stretching band, amide I and amide II modes) in the infrared spectra when organoclay was present in the matrix.[14,15] However, as nanoclay is known to induce crystallization in semicrystalline polyamides,[16] it was difficult to determine whether these changes were due to polymer–clay interactions or to changes in the crystalline phase.[17]

Besides hydrogen bonding, specific interactions, such as ionic interactions and van der Waals forces, can also provide attraction between the nanoclay layers and polymer matrix.[9,18] Usuki et al.[19] synthesized intercalated compounds of clay minerals with glycine as a model of *in situ* polymerized polyamide 6 nanocomposites. ^{15}N-NMR spectroscopy showed that the compound based on MMT had the most downfield resonance; this revealed that the positive charge density on the nitrogen of glycine in MMT was largest among all of the compounds. This suggested that for *in situ* polymerized polyamide 6 nanocomposites, the silicate layers could interact directly with the polymer molecules by strong ionic interaction.[19] It appeared that polyamide 6, because of its polarity or strong hydrogen-bonding ability, had some affinity for the pristine surface of the clay.[1] Lee and Han[9] investigated the phase behavior to compare the degree of compatibility between poly(vinyl acetate) and organoclay using cloud-point measurements. However, very little infrared investigation has been done on the characterization of different types of polymer–clay interaction besides hydrogen bonding.

Although most of the literature is focused primarily on the changes in the FTIR spectra of the polymer matrix in the presence of nanoclay, very little work has been reported on the corresponding changes in the nanoclay vibrational peaks, which would indicate definitively the existence of polymer–clay interactions. This is because, generally, the infrared vibrations of the Si—O stretching modes in MMT are rather difficult to resolve because of strong overlap with the polymer peaks.[20] These Si—O stretching bands, which show strong absorption in the range 900–1200 cm^{-1}, have been found to be very sensitive to the distortion of the tetrahedral structure and, hence, could be used to indicate the presence of polymer–clay interactions.

Recently, we prepared a novel amorphous semiaromatic polyamide/MMT nanocomposite based on poly(hexamethylene isophthalamide) (aPA) by melt intercalation.[21] By the suitable choice of organoclay, well-exfoliated morphologies were achieved in this system. The objective of this study was to use VT–FTIR spectroscopy to characterize important molecular interactions under the influence of nanoclay in the polymer matrix.

TABLE I
Material Properties of the Nanoclays and Surfactants Used in this Study

Nanoclay	Supplier designation	Specifications
NaMMT	Cloisite Na^+	CEC = 92.6, d_{001} spacing = 1.05 nm
30BMMT	Cloisite 30B: Methyl, tallow, bis-2-hydroxyethyl Quaternary ammonium chloride organoclay	CEC = 90, organic content = 28.4 wt % d_{001} spacing = 1.84 nm
10AMMT	Cloisite 10A: Dimethyl, benzyl, hydrogenated tallow Quaternary ammonium chloride organoclay	CEC = 125, organic content = 36.9 wt % d_{001} spacing = 1.95 nm

CEC, cation-exchange capacity (mequiv/100 g).

EXPERIMENTAL

aPA pellets were obtained from Lanxess (Singapore) under the product trade name Durethan T40. Durethan T40 is a completely amorphous polyamide.

Pristine sodium montmorillonite (NaMMT) nanoclay and two types of MMT-based organoclay were supplied by Southern Clay Products (Gonzales, Texas). They are abbreviated as NaMMT, 30BMMT, and 10AMMT, respectively. The chemical names of the surfactants are given in Table I. Before we blended the polymer and nanoclay, they were first dried in a vacuum oven at 80°C for at least 12 h. 1,1,1,3,3,3-Hexafluoro-2-propanol (HFIP; 99.8% purity) was purchased from Sigma-Aldrich (Singapore) and was used as received.

The polymer/clay nanocomposites were prepared via a two-step melt blending process with a Haake Polydrive (Germany) mixer in a nitrogen atmosphere according to the method described in a previous article.[21] For the aPA-containing nanoclay, polymer nanocomposites with nominal contents of 5 and 10 wt % MMT (the weight percentage excludes surfactants) were prepared. The pure aPA and polymer nanocomposites were then compressed into films (ca. 150 ± 5 μm thick) at 220°C with a Carver (Wabash, Indiana) press (model 4128).

Wide-angle X-ray diffraction (WAXD) measurements were performed at room temperature on a Siemens (Germany) D5005 X-ray diffractometer with Cu Kα radiation (λ = 0.1542 nm). The scanning rate was 1°/min for values of 2θ between 1 and 10°.

TEM was used to observe the dispersion of clay layers in the polymer matrix. Thin sections of 50 nm in thickness were cut from the nanocomposites at room temperature with a Leica (Germany) ultramicrotome with a diamond knife. The sections were then examined with a JEOL 3010 TEM instrument at an acceleration voltage of 200 kV.

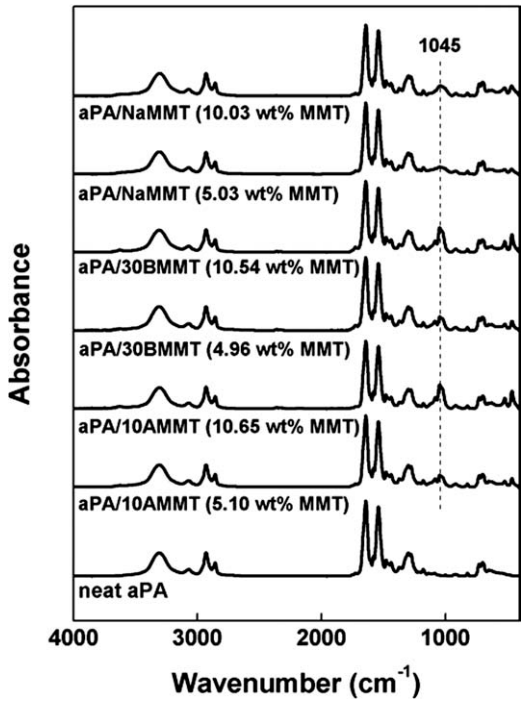

Figure 1 Room-temperature FTIR spectra of aPA and its nanocomposites.

VT–FTIR spectra were recorded with a deuterated triglycine sulfate detector on a Nicolet (Germany) model 5700 spectrometer equipped with a variable-temperature cell. The resolution was 2 cm^{-1}. A dry nitrogen purge was used to minimize absorption due to water. For infrared analysis, the polymer/nanoclay nanocomposites were first dissolved in HFIP to form a 2 wt % solution. From this solution, a film was prepared by solvent casting onto a KBr window. After evaporation of the majority of the solvent at room temperature, the KBr window with the film was placed in a vacuum oven at 80°C for at least 24 h to remove any residual solvent. The KBr window was then immediately transferred to the variable-temperature cell placed in the infrared spectrometer. The sample was first heated to 230°C at a heating rate of 20°C/min and then cooled to room temperature at a cooling rate of 10°C/min. FTIR spectra were recorded during the cooling run. At each temperature, the cell was equilibrated for at least 3 min before data collection. All of the samples used in this study were sufficiently thin to be within the absorbance range where the Lambert–Beer law was obeyed. The curve fitting of the spectra was carried out with Originlab (Northampton, Massachusetts) 7.5 software to determine the position, height, and area of each peak.

VT–FTIR spectra were also obtained for pure nanoclay powder as a control. A suspension containing 2 wt % nanoclay in HFIP was first cast onto a KBr window. After most of the solvent was evaporated at room temperature, the sample was heated to 230°C at a heating rate of 20°C/min in the FTIR spectrometer to remove the residual solvent. The sample was then cooled to room temperature at a cooling rate of 10°C/min. FTIR spectra were then recorded during the cooling run as before.

RESULTS AND DISCUSSION

The morphologies of the aPA/30BMMT, aPA/10AMMT, and aPA/NaMMT polymer nanocomposites prepared by melt intercalation were reported previously.[21] For all aPA/30BMMT nanocomposites, the WAXD pattern did not show any peaks; this indicated a fully delaminated and well-dispersed nanoclay morphology. This was confirmed by the TEM images. In the aPA/10MMT nanocomposites, an exfoliated morphology was obtained at the 5 wt % MMT loading, but a mixed exfoliated/intercalated morphology was obtained at the 10 wt % MMT content. The worst dispersion was observed for both aPA/NaMMT hybrids. WAXD and TEM indicated that the nanoclay particles agglomerated together.

Figure 1 shows the infrared spectra of aPA and its nanoclay nanocomposites recorded at room temperature in the range 400–4000 cm^{-1}. Table II lists the band assignments for aPA. The FTIR spectrum of aPA was characterized by three major groups: relatively strong bands were attributed to conformationally sensitive backbone modes, such as the amide modes and aliphatic hydrocarbon modes, and relatively weak bands were due to the conformationally insensitive modes of aromatic rings.[10] For purposes of this study, the focus was on the conformationally sensitive backbone modes. From Figure 1, it can be observed that at room temperature, the infrared spectra of all of the nanocomposites were fairly similar to that of aPA, except for the additional MMT bands at 3627, 1045, 520, and 462 cm^{-1}. They were attributed to bonded hydroxyl stretching, Si—O

TABLE II
FTIR Band Assignments of aPA at Room Temperature

Wavenumber (cm^{-1})	Band assignment
3309	Hydrogen-bonded N—H stretching (amide A)[156]
3069	Aromatic C—H stretching and Fermi resonance of NH stretching with the overtone of amide II
2932	Asymmetric CH_2 stretching
2858	Symmetric CH_2 stretching
1642	Amide I mode
1541	Amide II mode
1299	Amide III mode
1000	Metasubstituted aromatic vibration
700	Amide V mode
650	N—C=O in-plane bending[224]

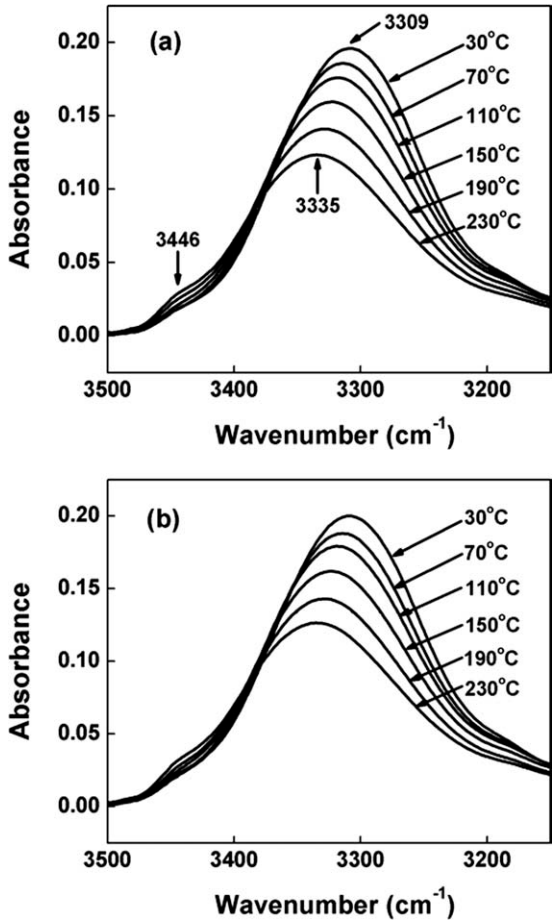

Figure 2 FTIR spectra of the N—H stretching region of (a) neat aPA and (b) aPA/30BMMT with 5 wt % MMT from 30 to 230°C.

stretching, Si—O—Al^{3+} deformation, and Si—O—Si deformation, respectively.[20]

N—H stretching band

The primary intermolecular interaction occurring in aPA homopolymer is the hydrogen bonding between the amide N—H group and the C=O group.[11] The band envelope encompassing the N—H stretching mode is composed of two main contributions, which are attributed to free (non-hydrogen-bonded) and hydrogen-bonded N—H groups.[10] Infrared spectroscopy has demonstrated that over 99% of N—H groups in both semicrystalline and amorphous polyamides are hydrogen-bonded to the C=O groups.[22] The frequency of the hydrogen-bonded N—H stretching mode reflects the average strength of the bonded N—H groups. On the other hand, the breath of this mode primarily reflects the distribution of hydrogen-bond distances and geometries.[17]

Figure 2(a) shows that the room-temperature (30°C) N—H stretching peaks of aPA exhibited two infrared bands at 3446 cm^{-1} (weak shoulder) and 3309 cm^{-1} (broad peak). These peaks were assigned to the free and hydrogen-bonded N—H stretching modes, respectively. The center frequencies of the hydrogen-bonded bands remained essentially constant in all of the nanocomposites; this implied that the average strength of the hydrogen-bonded N—H species was generally unaffected by the presence of both agglomerated NaMMT and well-dispersed 10AMMT and 30BMMT.

The N—H stretching bands of aPA/NaMMT and aPA/10AMMT with 5 wt % MMT had similar full width at half-maximum ($W_{1/2}$) values as the homopolymer. However, the peak width of aPA/30BMMT with 5 wt % MMT was observed to be slightly larger than that of the pure polymer; this indicated that the incorporation of 30BMMT broadened the distribution of the hydrogen-bonded N—H groups. Similar phenomena were also observed in the nanocomposites containing 10 wt % 30BMMT.

Figure 2 shows the effect of the temperature on the spectra of neat aPA and aPA/30BMMT with 5 wt % MMT. The spectra are shown on an absolute absorbance scale. The changes in the N—H stretching bands for the homopolymer and the hybrids had similar trends. As the temperature increased, the peak maxima shifted to high frequencies and the peak areas decreased. This indicated that the average strength of the hydrogen bonds decreased with increasing temperature.[10]

Figure 3 shows the graph of the N—H stretching peak shift (relative to the respective peak frequency at 30°C) versus the temperature for aPA and the nanocomposites containing 5 wt % MMT. All the peak shifts increased monotonically with temperature. Furthermore, the extent of peak shift was similar in all of the materials; this implied that both the NaMMT nanoclay agglomerates and the 10AMMT and 30BMMT nanoclay platelets did not significantly

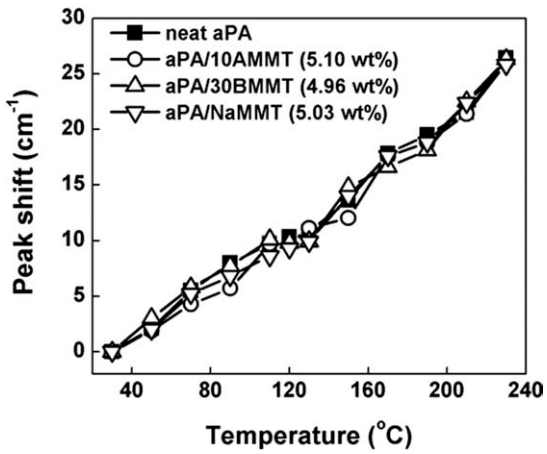

Figure 3 Peak shift of the N—H stretching band versus temperature for aPA and the nanocomposites.

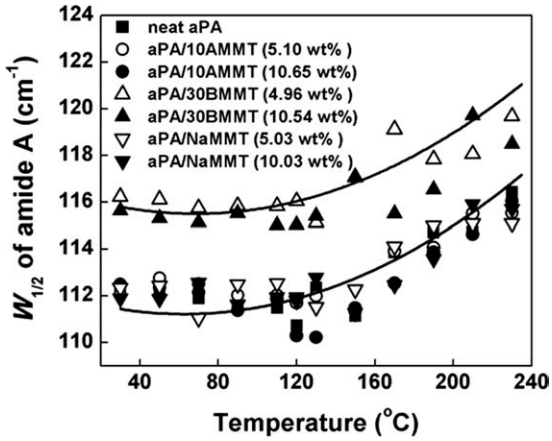

Figure 4 $W_{1/2}$ of the hydrogen-bonded N—H stretching peak (amide A) versus temperature for aPA and the nanocomposites. The two curves serve as a guide to the eye.

affect the stability of hydrogen bonding in the nanocomposites.

With a curve-fitting procedure, as described by Skrovanek et al.,[10] the frequencies of the free N—H stretching band and the peak width of the bonded N—H stretching (amide A) band were determined for aPA and its nanocomposites. The curve-fitting results show that for neat aPA, the peak position of free N—H stretching remained constant at 3446.0 cm^{-1} in the entire temperature range from 30 to 230°C. The amount of bonded N—H groups also remained unchanged at 99%. These results were consistent with literature reports.[10,22] Hence, even though the intensity of the N—H stretching band in aPA was observed to decrease with increasing temperature [Fig. 2(a)], there was no reduction in the number of bonded N—H groups. This observation was consistent with the results of Skrovanek et al.,[10] who attributed this reduction in intensity primarily to a decrease in the absorption coefficient of the N—H peak as the hydrogen bond strength decreased. Upon the incorporation of 10AMMT, 30BMMT, and NaMMT into aPA, similar phenomena were also observed for the peak position of the free N—H stretching band and the fraction of hydrogen-bonded N—H groups.

Figure 4 shows how the peak width of the bonded N—H stretching (amide A) band changed with the temperature for aPA and the nanocomposites. It was observed that the peak width generally increased with temperature in all of the samples. The band of the aPA/30BMMT system was always broader than those of other hybrid systems at all temperatures. For any given nanofiller, $W_{1/2}$ of the N—H peak remained fairly constant at both 5 and 10 wt % MMT; this indicated a similar distribution of hydrogen-bond distances and geometries, regardless of nanofiller content.

CH_2 stretching bands

Although the N–H stretching mode could be correlated to changes in the hydrogen-bond environment, the CH_2 asymmetric [$\nu_{as}(CH_2)$] and symmetric [$\nu_s(CH_2)$] stretching peaks were used to probe changes in the van der Waals interactions of the polymer nanocomposites.

Figure 5 shows the peak shifts of the $\nu_{as}(CH_2)$ bands with temperature for the aPA nanocomposites. At room temperature, as for the $\nu_s(CH_2)$ stretching band, the peak centers of the $\nu_{as}(CH_2)$ bands for aPA/30BMMT and aPA/NaMMT were similar to that of the homopolymer (2931.7 cm^{-1}), although the peak centers for aPA/10AMMT decreased with increasing nanoclay content. In aPA/10AMMT containing 5 wt % MMT, the peak center of the $\nu_{as}(CH_2)$ band was 2931.5 cm^{-1}, although at 10 wt % MMT, the peak center dropped further to 2931.2 cm^{-1}. As the temperature increased, the $\nu_{as}(CH_2)$ band shifted toward lower frequencies for all of the materials. Even though the frequency shifts appeared to be relatively small, they were reproducible to at least ± 0.1 cm^{-1}. The rate of decrease was similar for all of the systems. As temperature increased, there was a negligible frequency shift in the $\nu_s(CH_2)$ band for all of the samples.

VT–FTIR spectra of the MMT bands

Figure 6 shows the spectra of the organoclay 10AMMT and 30BMMT and pristine NaMMT dry powders in the Si—O stretching region from 960 to 1150 cm^{-1} at room temperature. All of the spectra were normalized to unit height. After the convention of Yan et al.,[23] the four Si—O stretching modes were labeled I, II, III, and IV, respectively. The peak at 1080 cm^{-1} represented an out-of-plane (perpendicular) vibration mode, whereas the other three peaks

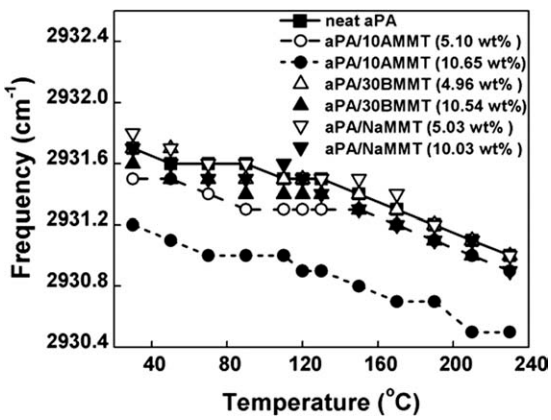

Figure 5 Graph of the peak center frequency versus temperature of the $\nu_s(CH_2)$ bands for aPA and its nanocomposites.

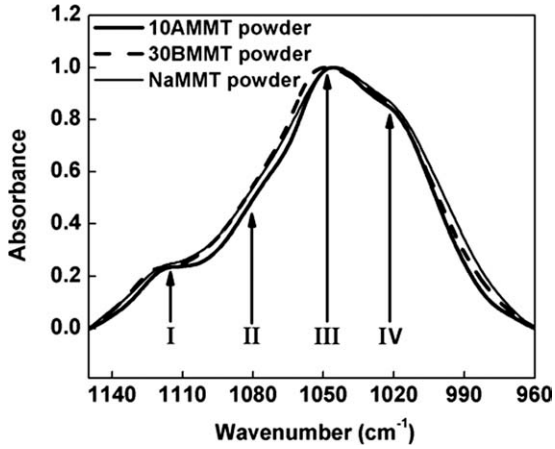

Figure 6 FTIR spectra in the Si—O stretching region from 1150 to 960 cm^{-1} of organoclay 10AMMT, 30BMMT, and pristine NaMMT powders normalized by height.

at 1110, 1050, and 1025 cm^{-1} represented in-plane (parallel) vibrations.[20,24]

Figure 7 shows the VT–FTIR spectra in the Si—O stretching region for the aPA/10AMMT, aPA/30BMMT, and aPA/NaMMT nanocomposites at a 5 wt % MMT loading. As the strong Si—O peaks overlapped with some weak aPA peaks, the pure Si—O stretching peak at each temperature was obtained by a simple spectrum subtraction procedure discussed previously.[21] It can be observed from Figure 7 that the Si—O stretching peaks shifted to lower frequencies with increasing temperature. Furthermore, all of the maximum peak intensities also increased with temperature. Similar phenomena were also observed for the hybrids containing 10 wt % MMT.

Figure 8 shows the peak shifts (relative to the respective peak maximum at 30°C) versus temperature for the Si—O stretching absorption of the pure nanoclay powder and the nanocomposites. The peak position was taken to be the location of the maximum peak height in the Si—O stretching region of each spectrum. From Figure 8(a), the extent of peak shift in all of the nanoclay powders and aPA/NaMMT was similar. However, Figure 8(b) shows that significant peak shifts were observed in both the aPA/10AMMT and aPA/30BMMT nanocomposites. The Si—O stretching absorptions of aPA/10AMMT and aPA/30BMMT shifted by approximately 10 cm^{-1} as the temperature increased from 30 to 230°C, compared to the lower 5–6-cm^{-1} shift in the 10AMMT and 30BMMT powders.

Nature of the matrix–nanoclay interactions

Hydrogen-bonding interactions

Polyamides are strongly self-associating through intermolecular hydrogen bonding. As mentioned in the Introduction section, in the studies of other semicrystalline polyamide/nanoclay nanocomposites, the frequencies of the N—H peaks were observed to shift upon introduction of nanoclay into the polymer.[14,,15] Furthermore, VT–FTIR studies of semicrystalline polyamide 6 and polyamide 66 and their nanocomposites have shown that the change rates of peak frequency and intensity with increasing temperature were considerably less than those of the homopolymers.[8,25] These observations were attributed to the greater stability of hydrogen

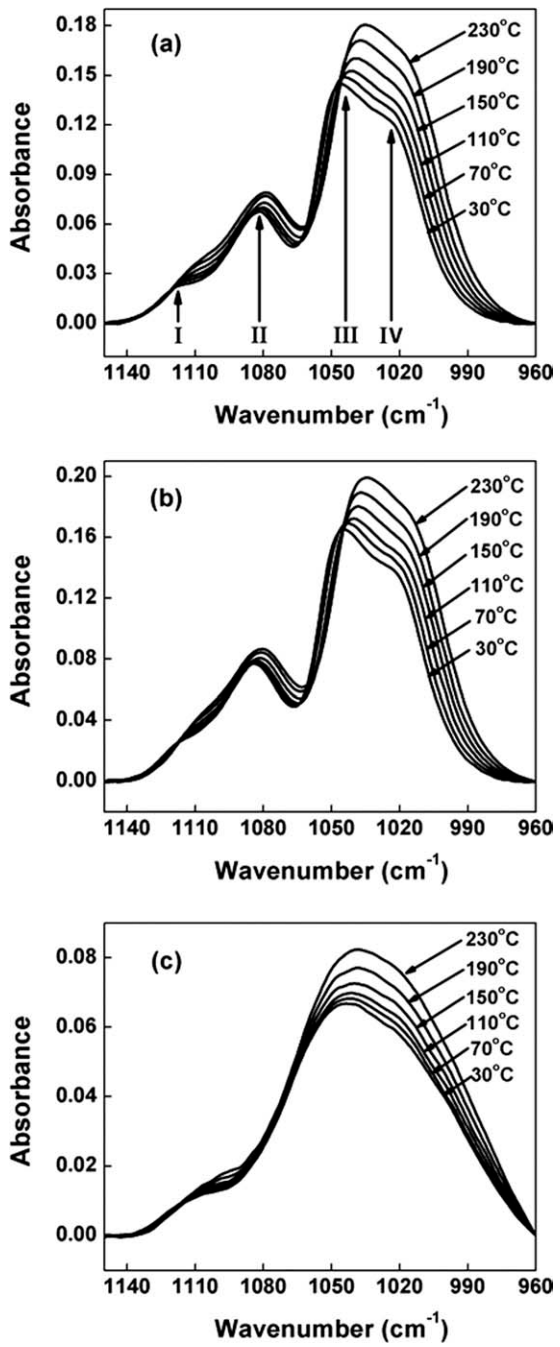

Figure 7 VT–FTIR spectra in the Si—O stretching region for (a) aPA/10AMMT, (b) aPA/30BMMT, and (c) aPA/NaMMT nanocomposites at 5 wt % MMT loading.

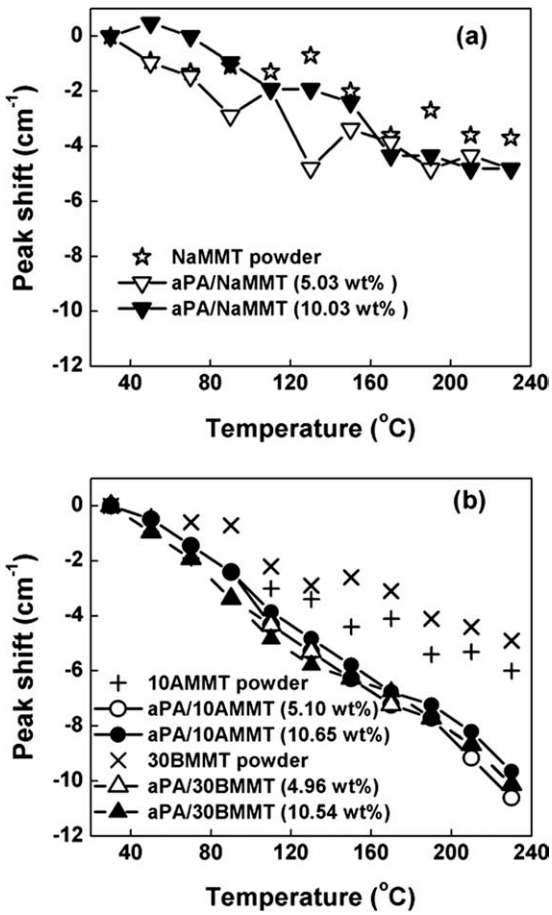

Figure 8 Peak shift versus temperature for the Si—O stretching absorptions of the (a) NaMMT powder and aPA/NaMMT hybrids and (b) organoclay powders and aPA/organoclay nanocomposites.

bonding between the polymer and nanoclay in the hybrids.

The FTIR results for the aPA nanocomposites showed a completely different behavior. In the aPA/NaMMT system, the infrared absorptions of the polymer matrix were not influenced by the addition of pristine clay. This indicated that little interaction existed between the polymer chains and the hydrophilic surface of the MMT.[25] In a similar fashion, the FTIR results also showed that the presence of exfoliated 10AMMT nanofillers had little effect on the intermolecular hydrogen-bonding environment of the aPA matrix. This implied that in the aPA nanocomposites prepared by melt intercalation, it was difficult for the polymer chains to come into contact directly with the nanoclay surface to form strong hydrogen bonding and that the main interfacial attraction was between the polymer and the surfactant.[18]

Hence, the changes in the amide bands that have been observed in semicrystalline polyamide nanocomposites should be primarily attributed to a nanoclay-induced crystalline phase rather than to polymer–clay interactions. In our work, the completely amorphous nature of aPA in the nanocomposites allowed for a more straightforward interpretation of the infrared data. In semicrystalline polyamides, not only do the amide bands of the crystalline phase overlap with those of the amorphous phase, it is also very difficult to resolve them; this, thereby, introduces complications in interpreting the spectra.

The infrared spectra showed that with the addition of the organoclay 30BMMT, the N—H stretching bands showed an increase in bandwidth. This indicated that the well-dispersed 30BMMT clay platelets disrupted the self-associated hydrogen bonding between polymer chains and formed new hydrogen bonds with amide moieties on aPA so as to broaden the distribution of hydrogen bonding.[26]

The curve-fitting results show that the fraction of free N—H groups in aPA/30BMMT still remained constant, even at a high filler loading with increasing O—H concentration. This indicated the existence of a balance between the disruption of polymer self-associated hydrogen bonds and the formation of new hydrogen bonds with 30BMMT. Therefore, any excess organic nanoclay could not provide further sites, that is, O—H groups, to form more hydrogen-bonding interactions with the polymer chains.[11] On the contrary, the addition of more nanofillers tended to increase the degree of phase heterogeneity in the polymer nanocomposites. Hence, there always exists an optimal nanoclay content for property enhancement, such as improved mechanical properties and thermal stability, in polymer/nanoclay systems.[27]

Non-hydrogen-bonding interactions

The frequency, width, and intensity of CH_2 stretching bands in small molecules are sensitive to the gauche/trans conformer ratio of the methylene chains and the intermolecular interactions between the organic chains.[28] With increasing trans-order structure, $\nu_{as}(CH_2)$ shifts to lower frequencies. The behavior and properties of polymer/organoclay hybrids depend largely on the structure and molecular environment of the intercalated organic surfactant between clay galleries.[28] Before we can explain the decrease in the frequency of the CH_2 stretching bands in the aPA/10AMMT system at room temperature, it is necessary to study the FTIR results of the organic surfactants on 10AMMT and 30BMMT at room temperature, for infrared spectroscopy has been widely used to directly probe the molecular conformation of intercalated chains and provide better insight into the interlayer structure of the nanoclay–organic surfactant system.[28]

Figure 9 shows the room-temperature infrared spectra of the aliphatic CH_2 stretching bands of the 10AMMT and 30BMMT powders. All of the spectra

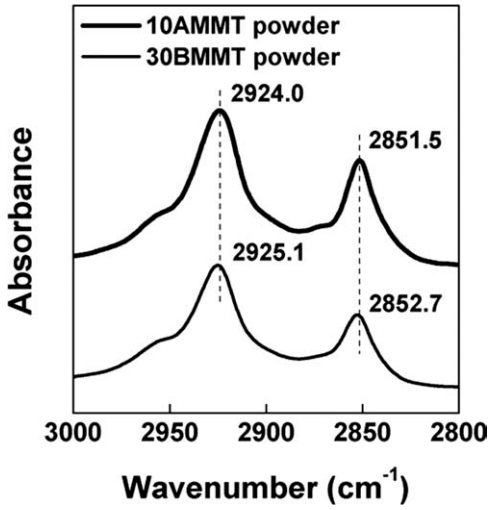

Figure 9 Room-temperature FTIR spectra of the aliphatic C—H stretching region of 10AMMT and 30BMMT powder in the range 3000–2800 cm^{-1}.

were normalized on the basis of the Si—O stretching band. It was observed that the frequency of $\nu_{as}(CH_2)$ of the 10AMMT powder was lower than that of 30BMMT; this implied a more ordered trans structure in the molecular environment of the 10AMMT interlayer.

It was demonstrated for organoclay that an increased trans conformation (increased order) of the surfactant would result in a more solidlike state of the organoclay interlayer, whereas an increased gauche conformation (increased disorder) implied a more liquidlike state.[28] In the aPA/10AMMT nanocomposites, the solidlike interlayer structure in the 10AMMT organoclay led to increased contact with the surrounding polymer chains; this resulted in more cohesive van der Waals interactions between the phenyl rings on 10AMMT and the aromatic moieties in the polymer.[18,27] Hence, in the aPA/10AMMT system, the shift toward lower frequencies for the asymmetric CH_2 stretching band at room temperature indicated a more stable molecular structure of the polymer chains upon the introduction of the 10AMMT organoclay and enhanced compatibility between the polymer and the organoclay.[28]

Effect of the matrix–nanoclay interactions

For the nanoclay infrared bands, Si—O stretching peak shifts to lower frequencies were observed before in polyamide 6/MMT as a result of stress transfer from the polymer matrix to the nanoclay platelets.[24] Yan et al.[23] also observed Si—O peak shifts in water–nanoclay systems. The Si—O stretching peaks became weaker in intensity and shifted to higher frequencies as the mass ratio of water to clay increased. These changes were attributed to the formation of stronger and shorter hydrogen bonds as more water penetrated between the individual clay layers. It was proposed that the existence of hydrogen bonding between the basal oxygen atoms of the silica tetrahedral and water molecules and the internal interactions were strong enough to result in mutual structural modification. Hence, the Si—O stretching vibrations in the MMT layers were assumed to be coupled to the H—O—H bending vibrations in the interlayer water.

In the aPA/nanoclay nanocomposites, because no external force was applied, the Si—O peak shifts in the nanoclay powders and in aPA/NaMMT were attributed to structural changes in the nanoclay as a result of increasing temperature. The larger peak shifts in the aPA/10AMMT and aPA/30BMMT nanocomposites were due to both changes within the nanoclay and changes in the weak interactions between the layered silicate and the polymer. As the temperature increased, the interfacial attractions between the clay and polymer chains were weakened; this contributed to a negative peak shift in the Si—O stretching band and an increase in the peak intensity. This was consistent with the observations of Yan et al.[23]

From Figure 8(b), it is possible to express the linear relationship between the peak shift of the Si—O stretching band and temperature with the following equation:

$$\Delta\nu_{Si-O} = AT + B \quad (1)$$

where $\Delta\nu_{Si-O}$ is the frequency shift of the Si—O stretching band, T is the temperature, and A and B are parameters obtained from the best fit straight line. The values of these parameters depend on the nature of the polymer nanocomposite.

Table III lists the values of A and B. In the aPA/30BMMT nanocomposites, the values of A were similar, regardless of the MMT content. However, for the aPA/10AMMT hybrids, there was a difference between the values of A for the 5.10 and 10.65 wt % MMTs. This was because the 30BMMT organoclay was well-dispersed in the polymer matrix even at high MMT loading, whereas the presence of intercalated clay layers in aPA/10AMMT at high clay

TABLE III
Statistically Determined Parameters from Equation (1)

	A	B	R^2
aPA/10AMMT			
5.10 wt %	−0.0537	1.984	0.9912
10.65 wt %	−0.0487	1.723	0.9940
aPA/30BMMT			
4.96 wt %	−0.0493	1.326	0.9946
10.54 wt %	−0.0486	1.197	0.9857

loading reduced the amount of favorable interactions between the polymer and the organoclay surface.[1] Hence, *A* was the parameter that reflected the extent of changes in the interfacial interactions with increasing temperature.

CONCLUSIONS

VT–FTIR spectroscopy was able to demonstrate, for the first time, interactions at the interface of layered silicate in polymer/nanoclay nanocomposites. Changes in the Si—O stretching vibrations in the nanoclay were attributed to a weakening of interfacial interactions. VT–FTIR spectroscopy also revealed the nature of the polymer–surfactant interactions. For organoclays containing quanternary amine surfactants with hydroxyl groups, the polymer formed hydrogen bonds with the amide N—H and C=O moieties on the polymer chains. Organoclays with surfactants containing phenyl groups also led to improved compatibility with the semiaromatic polymer matrix. The behavior of the N—H stretching band with temperature indicated that the polymer–nanoclay interactions were weak. This study demonstrated the utility of VT–FTIR spectroscopy in probing interfacial phenomenal in polymer nanocomposites.

The authors thank Mary Chan and Tan Ruoshan for the use of their materials and equipment.

References

1. Fornes, T. D.; Hunter, D. L.; Paul, D. R. Macromolecules 2004, 37, 1793.
2. Rao, Y. Q.; Pochan, J. M. Macromolecules 2007, 40, 290.
3. Kim, E. S.; Shim, J. H.; Woo, J. Y.; Yoo, K. S.; Yoon, J. S. J Appl Polym Sci 2010, 117, 809.
4. Fornes, T. D.; Paul, D. R. Macromolecules 2004, 37, 7698.
5. Kojima, Y.; Usuki, A.; Kawasumi, M.; Okada, A.; Kurauchi, T.; Kamigaito, O. J Polym Sci Part A: Polym Chem 1993, 31, 1755.
6. Beatrice, C. A. G.; Branciforti, M. C.; Alves, R. M. V.; Bretasi, R. E. S. J Appl Polym Sci 2010, 116, 3581.
7. Cole, K. C.; Denault, J.; Bureau, M. N. Macromol Symp 2004, 205, 47.
8. Lu, Y. L.; Zhang, G. B.; Feng, M.; Zhang, Y.; Yang, M. S.; Shen, D. Y. J Polym Sci Part B: Polym Phys 2003, 41, 2313.
9. Lee, K. M.; Han, C. D. Macromolecules 2003, 36, 7165.
10. Skrovanek, D. J.; Howe, S. E.; Painter, P. C.; Coleman, M. M. Macromolecules 1985, 18, 1676.
11. Coleman, M. M.; Skrovanek, D. J.; Hu, J. B.; Painter, P. C. Macromolecules 1988, 21, 59.
12. George, A. J.An Introduction to Hydrogen Bonding; Oxford: New York, 1997.
13. Lee, K. M.; Han, C. D. Polymer 2003, 44, 4573.
14. Lu, Y. L.; Zhang, Y.; Zhang, G. B.; Yang, M. S.; Yan, S. K.; Shen, D. Y. Polymer 2004, 45, 8999.
15. Nair, S. S.; Ramesh, C. Macromolecules 2005, 38, 454.
16. Lincoln, D. M.; Vaia, R. A.; Wang, Z. G.; Hsiao, B. S. Polymer 2001, 42, 1621.
17. Skrovanek, D. J.; Painter, P. C.; Coleman, M. M. Macromolecules 1986, 19, 699.
18. Jang, B. N.; Wang, D. Y.; Wilkie, C. A. Macromolecules 2005, 38, 6533.
19. Usuki, A.; Koiwai, A.; Kojima, Y.; Kawasumi, M.; Okada, A.; Kurauchi, T.; Kamigaito, O. J Appl Polym Sci 1995, 55, 119.
20. Farmer, V. C.; Russell, J. D. Spectrochim Acta 1964, 20, 1149.
21. Zhang, X., Bhuvana, S. and Loo, L. S. (2011) J. Appl. Polym. Sci. doi: 10.1002/app.36266.
22. Schroeder, L. R.; Cooper, S. L. J Appl Phys 1976, 47, 4310.
23. Yan, L. B.; Roth, C. B.; Low, P. F. Langmuir 1996, 12, 4421.
24. Loo, L. S.; Gleason, K. K. Macromolecules 2003, 36, 2587.
25. Zhang, X. K.; Yang, G. S.; Lin, J. P. J Polym Sci Part B: Polym Phys 2006, 44, 2161.
26. Yeh, J. T.; Yao, W. H.; Du, Q. G.; Chen, C. C. J Polym Sci Part B: Polym Phys 2005, 43, 511.
27. Zhang, X. G.; Loo, L. S. J Polym Sci Part B: Polym Phys 2008, 46, 2605.
28. Vaia, R. A.; Teukolsky, R. K.; Giannelis, E. P. Chem Mater 1994, 6, 1017.